Historical Trends in Ocean Heat, Carbon, Salinity, and Oxygen Simulations: Impact of a Changing Ocean Circulation

Scott Mannis[1], Darryn W. Waugh[1], Anand Gnanadesikan[1], and Thomas W N Haine[1]

[1]Johns Hopkins University

December 7, 2023

Abstract

Examination of historical simulations from CMIP6 models shows substantial pre-industrial to present-day changes in ocean heat (ΔH), salinity (ΔS), oxygen (ΔO2), dissolved inorganic carbon (ΔDIC), chlorofluorocarbon-12 (ΔCFC12), and sulfur hexafluoride (ΔSF6). The spatial structure of the changes and the consistency among models differ among tracers: ΔDIC, ΔCFC12, and ΔSF6 all are largest near the surface, are positive throughout the thermocline with weak changes below, and there is good agreement amongst the models. In contrast, the largest ΔH, ΔS, and ΔO2 are not necessarily at the surface, their sign varies within the thermocline, and there are large differences among models. These differences between the two groups of tracers are linked to climate-driven changes in the ocean transport, with this tracer "redistribution" playing a significant role in changes in ΔH, ΔS, and ΔO2 but not the other tracers. Tracer redistribution is prominent in the southern subtropics, in a region where apparent oxygen utilization and ideal age indicate increased ventilation time scales. The tracer changes are linked to a poleward shift of the peak Southern Hemisphere westerly winds, which causes a similar shift of the subtropical gyres, and anomalous upwelling in the subtropics. This wind - tracer connection is also suggested to be a factor in the large model spread in some tracers, as there is also a large model spread in wind trends. A similar multi-tracer analysis of observations could provide insights into the relative role of the addition and redistribution of tracers in the ocean.

Hosted file

980977_0_art_file_11644474_s4ydw0.docx available at https://authorea.com/users/705689/articles/691221-historical-trends-in-ocean-heat-carbon-salinity-and-oxygen-simulations-impact-of-a-changing-ocean-circulation

Historical Trends in Ocean Heat, Carbon, Salinity, and Oxygen Simulations: Impact of a Changing Ocean Circulation

S. Mannis, D. W. Waugh, A. Gnanadesikan, T. W. N. Haine

Department of Earth and Planetary Sciences, Johns Hopkins University

Corresponding author: Darryn Waugh (waugh@jhu.edu)

Key Points:

- Historical changes in DIC, CFC12, and SF_6 in CMIP6 simulations show similar spatial patterns and general agreement among the models.
- Historical changes in T, S, and O_2 show regional differences, including in sign, among tracers and a wide variation among the models.
- Increases in surface values dominate changes in DIC, CFC12, and SF_6, but changes in ocean transport are more crucial for T, S, and O_2.

Abstract

Examination of historical simulations from CMIP6 models shows substantial pre-industrial to present-day changes in ocean heat (ΔH), salinity (ΔS), oxygen (ΔO_2), dissolved inorganic carbon (ΔDIC), chlorofluorocarbon-12 (ΔCFC12), and sulfur hexafluoride (ΔSF_6). The spatial structure of the changes and the consistency among models differ among tracers: ΔDIC, ΔCFC12, and ΔSF_6 all are largest near the surface, are positive throughout the thermocline with weak changes below, and there is good agreement amongst the models. In contrast, the largest ΔH, ΔS, and ΔO_2 are not necessarily at the surface, their sign varies within the thermocline, and there are large differences among models. These differences between the two groups of tracers are linked to climate-driven changes in the ocean transport, with this tracer "redistribution" playing a significant role in changes in ΔH, ΔS, and ΔO_2 but not the other tracers. Tracer redistribution is prominent in the southern subtropics, in a region where apparent oxygen utilization and ideal age indicate increased ventilation time scales. The tracer changes are linked to a poleward shift of the peak Southern Hemisphere westerly winds, which causes a similar shift of the subtropical gyres, and anomalous upwelling in the subtropics. This wind - tracer connection is also suggested to be a factor in the large model spread in some tracers, as there is also a large model spread in wind trends. A similar multi-tracer analysis of observations could provide insights into the relative role of the addition and redistribution of tracers in the ocean.

Plain Language Summary

Changes in ocean properties can have a large impact on Earth's climate (e.g., ocean storage of heat and carbon) and biology within the oceans (e.g., acidification and deoxygenation). Here we examine historical changes in multiple ocean fields from an ensemble of climate model simulations. The spatial structure of the changes and the consistency among models differs between tracers. Dissolved inorganic carbon (DIC), chlorofluorocarbon-12 (CFC12), and sulfur hexafluoride (SF_6) all have largest increases near the surface, increase throughout the thermocline with weak changes below, and there is good agreement amongst the models. However, for ocean heat (H), salinity (S), oxygen (O_2) the largest changes are not necessarily at the surface, the sign of the change varies among tracers, and there are large differences among models. These differences between the two groups of tracers are linked to climate-driven changes in the ocean transport, with this tracer "redistribution" playing a significant role in changes in H, S, and O_2 but not the other tracers. A similar multi-tracer analysis of observations could provide insights into the relative role of the addition and redistribution of tracers in the ocean.

1. Introduction

Substantial changes in the oceans have been observed over the last few decades, including changes in temperature (Johnson et al. 2018, Cheng et al. 2022), salinity (Durack 2015, Cheng et al. 2020), carbon (McKinley et al. 2017, Gruber et al. 2023), and dissolved oxygen (Keeling et al. 2010, Breitburg et al. 2018). These changes in ocean properties have an impact on ocean circulation (through temperature and salinity changes), ocean biogeochemistry (acidification and deoxygenation), and Earth's climate (ocean storage of heat and carbon). It is therefore important to understand the cause of the changes and for models to be able to reproduce the changes.

There are multiple mechanisms that could cause the observed changes. One is changes in atmosphere-ocean surface fluxes, either through changes in the atmosphere (e.g. increased atmospheric temperature and carbon dioxide, or changes in precipitation) or temperature-driven changes in solubility of gasses. The resulting change in surface properties is then transported into the thermocline and deep ocean. This is often referred to as the passive transport of ocean tracers or the "added" component of tracer changes (e.g., Banks and Gregory 2006, Bronselaer and Zanna 2020). If this mechanism is the dominant cause of the changes in ocean properties, then the change in different properties would have very similar spatial distributions. However, several recent studies have shown substantial differences in the simulated distributions of anthropogenic heat and carbon storage (e.g., Frolicher et al. 2015, Williams et al. 2021). Specifically, while carbon increases throughout the thermocline, heat decreases in the low-latitude sub-surface thermocline. Further, while all models show a similar pattern of carbon storage, there is a large spread in the pattern of heat storage. This indicates passive transport is not the only mechanism controlling the distribution of these two tracers.

A second mechanism is climate-driven changes in the ocean circulation. These circulation changes act on the background tracer gradients to produce changes in the tracer distribution. This has been referred to as the "redistribution" of tracers (Winton et al. 2013, Bronselaer and Zanna 2020). The redistribution effect depends on the background gradients of the tracer, and so could differ in magnitude, and even in sign, between tracers (e.g., Williams et al. 2021). Although the added heat and carbon have a similar sign as the net source of both is increasing with time, the redistribution of heat and carbon can have differing signs due to the opposing gradients in the preindustrial temperature and carbon (e.g., Williams et al. 2021). Also the redistribution effect may be more prominent for heat than carbon because compensation between the solubility and biological carbon pumps reduces the sensitivity of air-sea carbon fluxes to changes in circulation (Marinov and Gnanadesikan, 2011).

While there appears to be consensus that the tracer "redistribution" is the cause of the differences in heat and carbon storage, there is large uncertainty in how the ocean transport has changed, what has caused these changes, and why there is such a large spread amongst models in their heat uptake. Furthermore, it is unclear what the balance between "added" and "redistributed" components is for other important ocean properties (e.g. salinity and oxygen), e.g., are the spatial patterns of change for these properties similar to carbon or heat, and is the spread among models large (as for heat) or small (as for carbon)?

Here we address these questions by examining changes in multiple ocean properties in Coupled Model Intercomparison Project Phase 6 (CMIP6) historical simulations (Eyring et al. 2016). This includes not only heat and carbon as considered in the above (CMIP5) studies, but also salinity (S), oxygen (O_2), chlorofluorocarbon-12 (CFC12), and sulfur hexafluoride (SF_6). These tracers have different surface histories and background gradients, so the impact of added and redistributed components will likely vary among the tracers, and comparison of the historical changes of a range of tracers may provide constraints on the circulation/transport changes. We also examine simulations of the ideal age tracer (Thiele & Sarmiento 1990, England 1994) that provide information on changes in ventilation (surface to interior transport) time scales, and can be used to identify regions where redistribution may be important.

The model output and analysis are described in the next section. In Section 3 we examine and compare the pre-industrial to present-day changes in the different fields, while in Section 4 we examine the mechanisms causing the change in circulation and tracers. Concluding remarks are in Section 5.

2. Methods

We examine the change in T, S, DIC, O_2, CFC12, SF_6, and ideal age within 18 CMIP6 historical simulations (1850-2014). All models have T, S, but only a subset have DIC, O_2, CFC12, SF_6, and ideal age, see Table 1. We use a single ensemble member for each model. For most models this is ensemble member ''r1i1p1f1'', but for some this member is not available, in which case we use another ensemble member, as listed in Table 1. To aid with interpretation of the results in oxygen, we have also calculated the apparent oxygen utilization (AOU), defined as the difference between the saturation oxygen concentration at the temperature and salinity at a given grid point and the modeled oxygen at that grid point.

Model output that are not on a regular 1x1 horizontal grid were interpolated onto this grid. Analysis of individual models was done on individual model vertical levels, but the output was interpolated onto a common vertical grid with 10 m resolution over the top 2000m for creation of multi-model mean fields.

The historical changes in each field are calculated as the difference between the time average over last 20 years and the time average over the first 20 years, i.e., $\Delta X = X_{1995\text{-}2014} - X_{1850\text{-}1869}$, where X=T, S, etc and $X_{1995\text{-}2014}$ is the average over 1995 to 2014. For most of the analysis we present the zonally-integrated or zonally-averaged fields, and focus on the large-scale features of the changes in tracers in latitude-depth space.

Model	**Variant**	**DIC**	**T**	**S**	**CFC12**	**SF_6**	**O_2**	**age**
ACCESS-ESM1-5	r1i1p1f1	X	X	X			X	160
CanESM5	r1i1p1f1	X	X	X			X	4344
CESM2	r1i1p1f1	X	X	X	X	X		4041
CESM2-WACCM	r1i1p1f1	X	X	X	X	X		3931
CMCC-ESM2	r1i1p1f1	X	X	X			X	
CNRM-ESM2-1	r1i1p1f2	X	X	X			X	
EC-Earth-Consortium.…	r1i1p1f1	X	X	X	X	X	X	239
GFDL-CM4	r1i1p1f1	X	X	X	X	X	X	
GFDL-ESM4	r1i1p1f1	X	X	X	X	X	X	
GISS-E2-1-G	r101i1p1f1	X	X	X				696
HadGEM3-GC31-LL	r1i1p1f3		X	X				0
IPSL-CM6A-LR	r1i1p1f1	X	X	X			X	629
MIROC-ES2L	r1i1p1f2	X	X	X			X	1242
MRI-ESM2-0	r1i1p1f1		X	X				0
NorESM2-LM	r1i1p1f1	X	X	X	X	X	X	1457
NorESM2-MM	r1i1p1f1	X	X	X	X	X	X	1145
UKESM1-0-LL (MOHC)	r1i1p1f2	X	X	X	X	X	X	0
UKESM1-0-LL (NIMS-	r13i1p1f2	X	X	X	X	X	X	0

Table 1: Model names, variant of historical run, and tracers included in each model (X = included, blank = not included). The value listed for age is the maximum age (in years) at the start of the historical simulation.

3. Ocean Tracers

3.1 Heat and Carbon

We first consider the historical uptake of heat and carbon in CMIP6 historical simulations. The historical change in the zonally-integrated DIC averaged over all CMIP6 simulations ("multi-model mean") increases throughout the thermocline (**Fig 1a)**. In contrast, the ΔH increases in some regions (e.g., near-surface waters) but decreases in others (in particular, the southern subtropical sub-surface ocean (~100-700 m) (**Fig 1b)**. These differences between ΔDIC and ΔH are very similar to that found for CMIP5 models, see figure 9a,b of Frolicher et al. (2015) (hereinafter F15). As discussed in the Introduction, this indicates that there is not passive transport of both tracers (or equivalently, the added component does not dominate the change in both tracers).

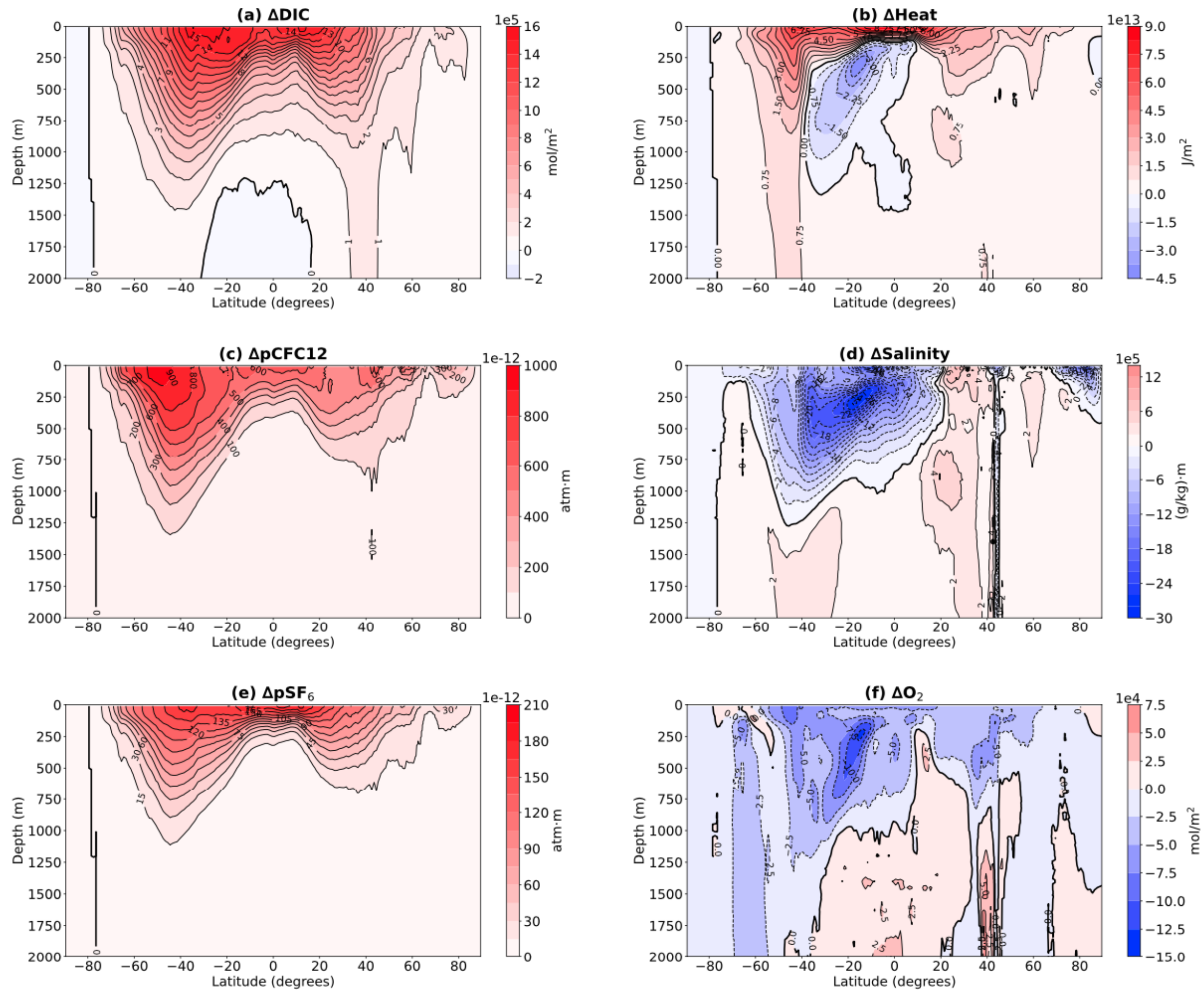

Figure 1: Depth-Latitude variations in multi-model mean zonally-integrated (a) ΔDIC (mol/m^2), (b) ΔH (J/m^2), (c) ΔCFC12 (atm.m), (d) ΔS (g/kg.m), (e) ΔSF_6 (atm/m), and (f) ΔO_2 (mol/m^2).

There is positive ΔDIC thoughout upper waters in all models, and all models show a very similar meridional variation and magnitude of the column-integrated ΔDIC, e.g., see **Fig. 2a** which shows the integrated ΔDIC over 100-700m. In contrast, there is a wide spread in ΔH among the models, with the difference not only in magnitude but also the meridional variations (**Fig 2b)**. This is again consistent with CMIP5 models, see, e.g., figures 2a and 6a of F15.

The disconnect between the uptake of C and H can also be seen by examining the relationship between ΔDIC and ΔH for each model. If both tracers were passively transported into the oceans, then models with larger ΔDIC would also have larger ΔH. However, this is not the case amongst CMIP6 models, and there is only a weak correlation between the ΔDIC and ΔH column inventories, e.g., **Fig. 3a** compares the 100-700m integral of ΔDIC and ΔH averaged over the southern subtropics (0-40^{o}S). (Although not shown in F15, a similar result is found for values in table 2 of F15.) As discussed in the Introduction, the above differences in ΔDIC and ΔH have been attributed to redistribution playing a major role in ΔH but not ΔDIC. This is discussed further in Section 4 below.

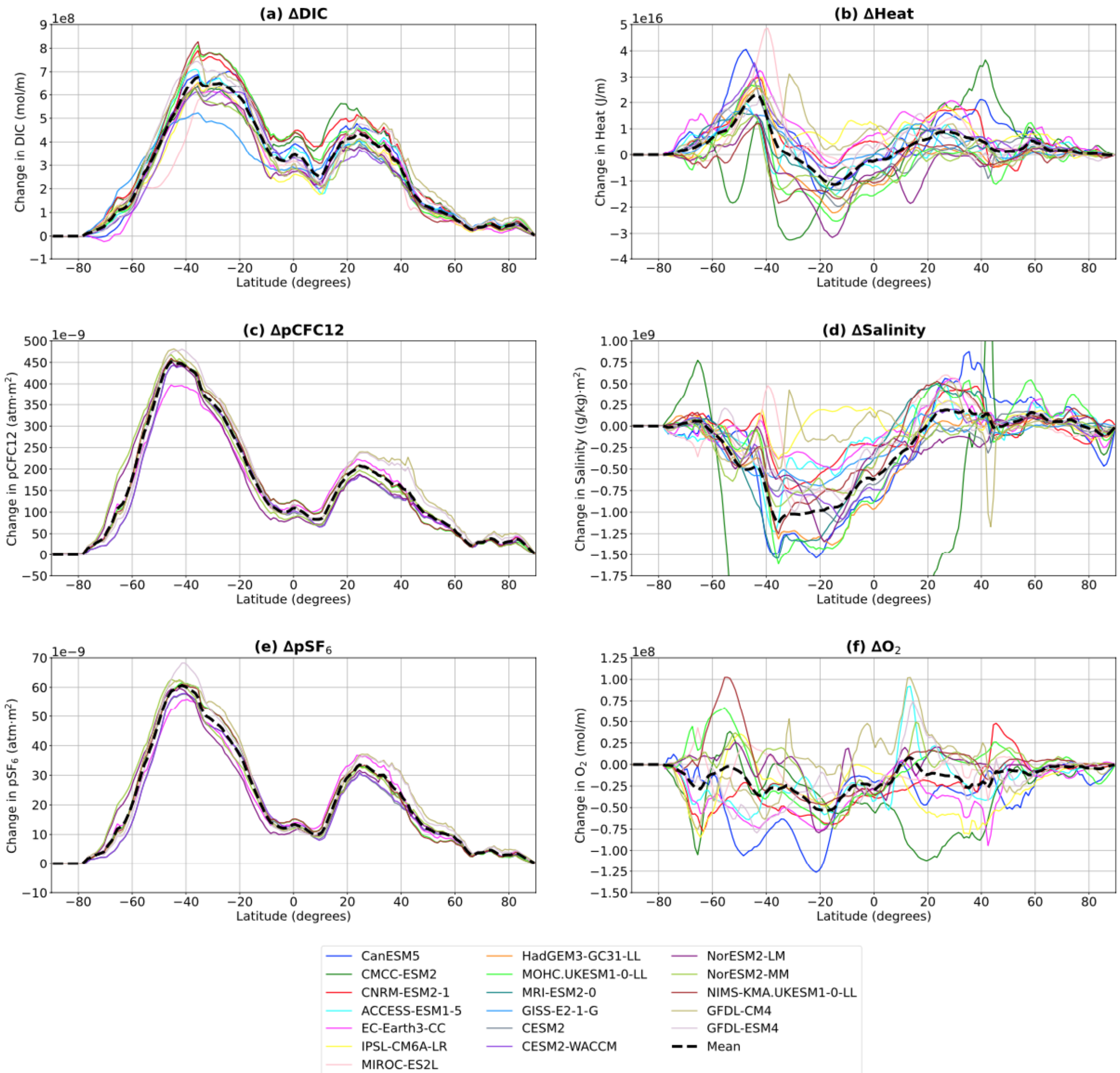

Figure 2: Latitudinal variation of the 100-700 m integrated column (a) ΔDIC, (b) ΔH, (c) ΔCFC12, (d) ΔS, (e) ΔSF_6, and (f) ΔO_2, for each model.

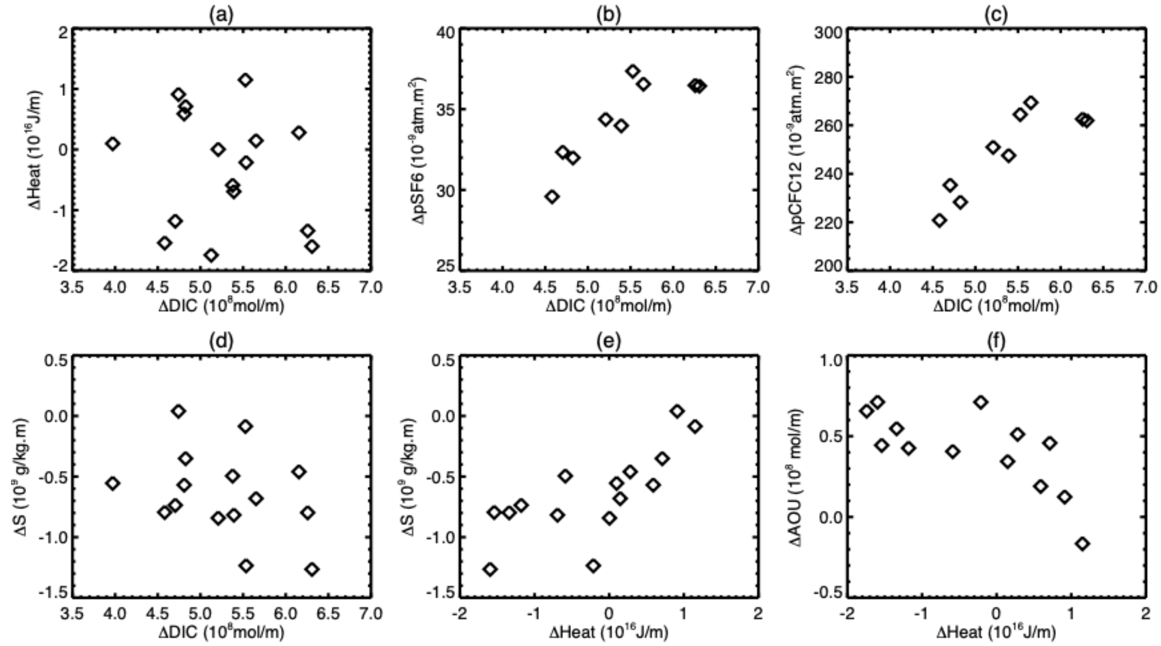

Figure 3: Relationships between (a) ΔDIC and ΔH, (b) ΔDIC and ΔpSF6, (c) ΔDIC and ΔpCFC12, (d) ΔDIC and ΔS, (e) ΔH and ΔS, and (f) ΔH and ΔAOU, for zonally-integrated 100-700m inventories averaged over 0-40S. Each symbol represents a different model.

3.2 Other Tracers

We next consider changes in CFC12 and SF_6. Both these gases are conserved in the oceans, have only anthropogenic sources, and their atmospheric concentrations have increased since the mid-20st century (Walker et al 2000). (There has been a decline in atmospheric CFC12 since the mid-1990s, due to the Montreal Protocol and amendments, but this decrease is small compared to the increase since the mid-20th century.) This results in increasing ocean surface concentrations from exchange with increased atmospheric concentrations that are transported into the subsurface oceans. As the pre-industrial atmospheric and ocean concentrations of CFC12 and SF_6 are zero, there are very weak background gradients at depth and redistribution by changes in transport will be small for these tracers, especially below the thermocline.

The multi-model mean patterns of ΔCFC12 and ΔSF_6 (which is equivalent to modern concentration as their pre-industrial levels are zero) are very similar, with large increases in the thermocline and negligible change at depth (**Fig. 1c, e**). (Note, we express these two tracers as partial pressure rather than concentration to avoid effects of temperature-driven changes in solubility.) The distributions of CFC12 and SF_6 are consistent with passive transport of the increasing surface concentrations into the ocean, with large values in regions with young ages (rapid ventilation) and vanishing values in the deep ocean where there are very old ages (slow ventilation).

The patterns of ΔCFC12 and ΔSF_6 are very similar to that of ΔDIC (**Fig. 1c,e**), and all models have very similar meridional distributions of upper-column ΔCFC12, ΔSF6, and ΔDIC (**Fig. 2a, c, e**). Furthermore, there are correlations across the models in the column-integrated ΔDIC, ΔCFC12, and ΔSF_6 (**Fig. 3b, c**), i.e., models that simulate a larger ΔCFC12 tend to simulate a larger ΔDIC (and ΔSF_6). The agreement among models in spatial variation, and a high correlation across models for these fields suggests that the impact of redistribution is much smaller than than that of of the passive transport or that it is potentially of the same sign as the "added component".

Next we consider salinity S. As with other tracers there are significant changes in S over the duration of the historical simulations. However, unlike the other tracers, ΔS is negative at the surface and throughout most of the thermocline (**Fig. 1d**), while small regions of positive change are seen in the North Atlantic. Salinification of the North Atlantic and freshening of the Pacific is consistent with the results of Durack (2015) and likely reflects an increase in interbasin freshwater transport coupled with a slowing of the overturning circulation. Additionally, we might expect polar regions supplying Southern Hemisphere intermediate waters to freshen as the hydrological cycle increases. However, the structure of ΔS indicates that the change is not simply the transport of this decrease into the interior (the "added" component). Unlike ΔDIC, ΔCFC12, and ΔSF_6, the largest change in southern low to mid-latitudes is not at the surface, but rather in the subtropical sub-surface (around 300 m, 20^{o}S). This region of large negative ΔS is similar to the region where there is negative ΔH (**Fig. 1b**), which suggests that redistribution may also be playing an important role for ΔS. Further, as for ΔH, there is a wide spread in ΔS among the models (**Fig. 2d**). In addition, there is a significant positive correlation across models for the 100-700 m ΔH and ΔS averaged between 0 and 40 ^{o}S (**Fig. 3e**), but no correlation between ΔDIC and ΔS (**Fig. 3d**). In other words, models that have a large decrease in H also have a large decrease in S. This supports the hypothesis that the same process (change in circulation) is causing the changes in S and H in this region.

The final realistic tracer we consider is oxygen O_2. The solubility of O_2 is temperature dependent, so the warming of the surface waters (which decreases the solubility) has caused a decrease in O_2 entering the oceans, and there is an "added'' component to ΔO_2 that we would expect to roughly track temperature with 10^{13} J/m^2 of heat gain being associated with around 0.12-0.15 x 10^5 mol/m^2 of oxygen loss. However, O_2 is not conserved within the oceans, and changes in this (biological) loss can cause non-zero ΔO_2. The spatial structure of the multi-model ΔO_2 shows decreases through most of the middle-upper oceans (**Fig. 1f**). The largest decreases are not at the surface, but in the southern, subtropical sub-surface ocean and in Antarctic waters. There is, moreover, a large spread amongst the models in upper-column ΔO_2 (**Fig. 2f**). These large changes in the subtropics and large model spread suggests that, as with H and S, changes in the ocean circulation have a large impact on ΔO_2.

From the above analysis we can separate the tracers into a group (DIC, CFC12, and SF_6) where there is good agreement amongst the models with all showing largest increase at the surface and an increase through the thermocline, and a second group (H, S, O_2) where there is a wide spread in simulated change amongst the models, including differences in sign of the change in some regions, and a region of large decrease in the southern subtropical sub-surface ocean.

A possible cause for this separation is differences in the relative role of the "added" and "redistribution" components to the tracer change, i.e., the change in the first group of tracers is dominated by the "added" component (with all tracers increasing because of the increase in atmospheric concentrations), whereas for the second group the redistribution effect plays a significant role, and there is a spread amongst the models in the simulated transport changes. For this to be the case there has to be a change in the tracer transport and for the tracer gradients to differ between the two groups. These aspects are examined the next sections.

3.3 AOU and Ideal Age

To quantify changes in the ocean transport we examine the changes in apparent oxygen utilization (AOU) and the ideal age tracer. Both of these quantities provide information on the timescales for transport from the ocean surface to interior, and whether these times have changed over the historical simulations.

AOU is the difference between oxygen gas solubility and the actual oxygen concentration, i.e., AOU = $O_{2,Sat}(T,S)$ - O_2, where $O_{2,Sat}$ is the saturated O_2, for given T and S. AOU depends on biological processes as well the transport times and pathways. However, if we assume the rate of biological loss is uniform throughout the ocean and does not change in time then AOU is proportional to the mean time scale for transport from the ocean surface. In general we expect the relationship between AOU and the mean transport time to be a strong function of depth, as remineralization of organic matter is strongly concentrated at the surface. Previous work (Bahl et al., 2019) has shown such correlations. However, at a given depth, it may be reasonable to use ΔAOU as a proxy for the change in the transport timescale from the surface to given location (this is tested below).

The multi-model mean ΔAOU shows a large increase in the southern subtropical region where ΔH and ΔS also decrease (**Fig. 4a**). Assuming constant biological loss, this increase in ΔAOU implies an increase in transport time from the surface (i.e. more time for the biology to consume O_2). As with ΔH and ΔS, there is a large spread in ΔAOU among the models (**Fig. 4b**). Furthermore, there is anti-correlation between ΔAOU and ΔH in southern low latitudes, i.e. models with larger increase in ΔAOU tend to have a larger decrease in ΔH (**Fig. 3f**), and there are strong similarities in the spatial variations of ΔAOU and ΔH in southern low-mid latitudes (see **Fig. 5** below). It is also worth noting that a 1 μM change in AOU would be expected to be associated with a 1.2-1.6 μM change in remineralized carbon. This means that if all of the ~1 x 10^5 mol m^{-2} decrease in oxygen along the equatorial edge of the Southern subtropical gyre in **Fig. 1f** is attributable to respiration, it would be associated with a ΔDIC about an order of magnitude smaller than the peak increase in **Fig. 1a**.

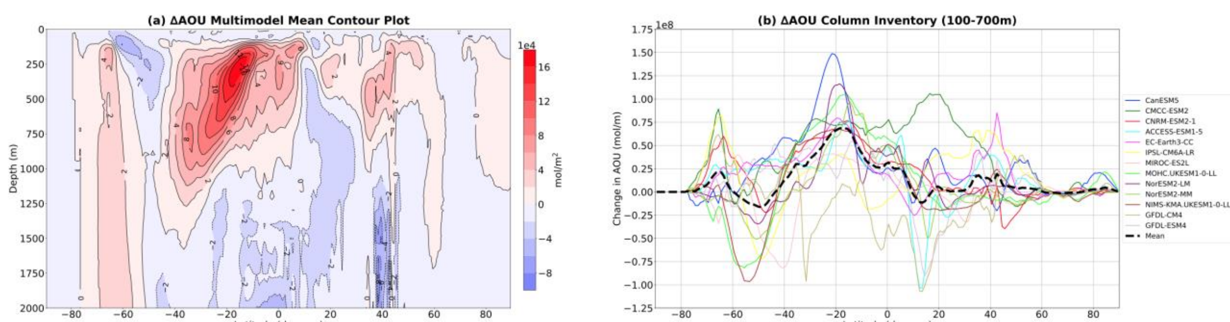

Figure 4 (a) Depth-Latitude variations in multi-model mean zonally integrated ΔAOU, and (b) 100-700m column inventory ΔAOU for each model.

The interpretation of ΔAOU as a change in transport times requires assumptions. A more direct measure of the transport times is the ideal age tracer (hereinafter referred to simply as the “age” or “age tracer”). In steady state, the age tracer is equal to the mean transport time from the surface to given interior location (Hall and Haine 2002), so Δage will quantify the change in the mean transport time from the surface.

Unfortunately, only a subset of the models includes the age tracer, and in many of these the age is not close to steady state. The latter can be seen by examining the maximum age at any ocean location at the start of the historical simulations, which is listed in Table 1. In steady state the maximum age should be well over 1000 yrs, however this is the case in only a few models. In some models the initial value in the historical simulations is zero (the age must have been reset at the start of the historical simulations), while for others the maximum age is only a few hundred years (the likely length of the pre-industrial simulation). The fact that the initial age is not in steady state means that Δage will include, and in many cases be dominated by, the increase in age as it approaches steady state, and not just be due to transport changes. Because of the above issue we consider only models with an initial maximum age over 600 years, so that the pre-industrial age is close to steady state, at least in waters above the main pycnocline. Further we do not calculate the multi-model mean change, as the impact of age approaching steady state varies between models due to very different initial ages.

Δage and ΔAOU for three models are shown in **Fig. 5**. In all models there is a decrease in age in southern mode-intermediate waters (above 500-1000m) and an increase in the age in southern subtropics (equatorward of 40 ^{o}S) around 500 m. However, the magnitude and exact region of these increases / decreases differs among the models. There are even larger differences occurring at depth, where Δage in some models is likely still approaching steady state. While there is not exact agreement between ΔAOU and Δage from the same model, there is agreement in the locations in the upper 1000m where ΔAOU and Δage increase or decrease, see **Fig. 5**. Furthermore, there are similar intra-model differences in ΔAOU and Δage, e.g., the decrease in ΔAOU and Δage around 40S is larger in NorESM2-LM than the other two models. There are some differences between ΔAOU and Δage at depth and near Antarctica that could be due to the above issue of age still approaching steady state.

The general agreement between ΔAOU and Δage for the few models that have usable age simulations indicates that ΔAOU from models can be used as an indicator of regions where there are changes in the ventilation time scale. Making this assumption, the simulated ΔAOU indicates that in all models there is an increase in ventilation time to the southern subtropical sub-surface region, but the exact location and magnitude of the change varies between models. Further, the variation between models in the location/strength of subtropical increase in ΔAOU (and Δage) is very similar to the variations in the decrease in ΔH among models, e.g., see **Fig. 5.**

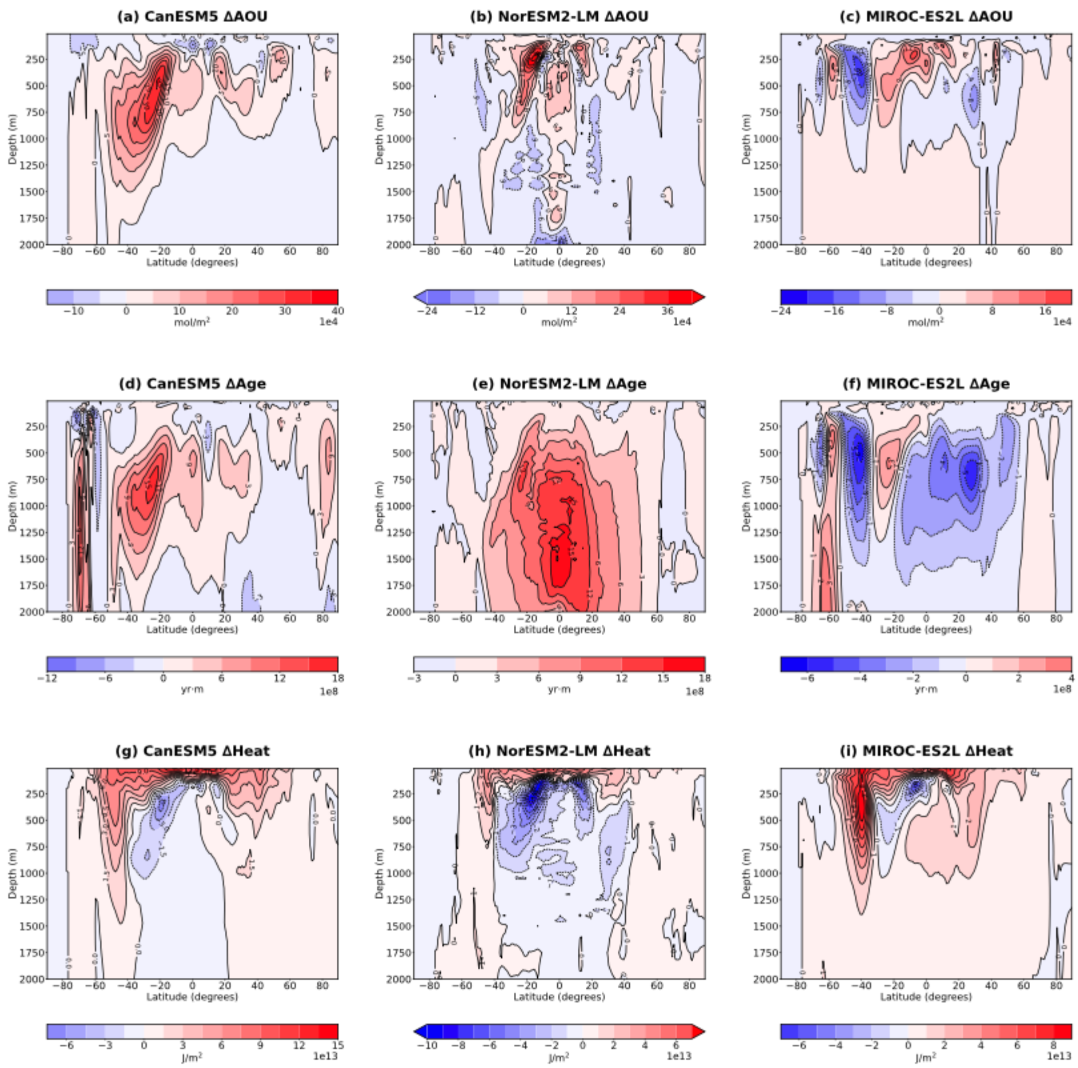

Figure 5. Depth-Latitude variations in (a-c) ΔAOU, (d-f) ΔAge, and (g-i) ΔH for the (left column) CanESM5, (middle) NorESM2-LM, and (right) MIROC-ES2L models.

4. Mechanisms

The above analysis suggests that there are changes in the ocean transport in the historical simulation that have a significant impact on ΔH, ΔS, and ΔO_2, but a much smaller impact on ΔDIC, ΔCFC12 and ΔSF_6. But there remain many questions and uncertainties. For example: How is the transport changing, what causes these changes, and why does its impact differ between tracers? Also, why is there a large spread in the change in transport and tracers amongst the models?

Fully answering these questions is beyond the scope of this study, but we present a preliminary analysis of the changes in the southern subtropical oceans. This is the region where, in most models, the largest increase in age occurs, and where H, S, and O_2 decrease, but DIC increases. Also, there is a large model spread in ΔH, ΔS, and ΔO_2 in the southern subtropics.

There are several mechanisms by which climate change can cause changes in ocean transport, including climate-driven changes in ocean temperature and salinity as well as atmospheric wind forcing (e.g., Clement et al. 2022, Newsom et al. 2022). The latter is potentially important for changes in the southern subtropical oceans as there has been a poleward shift and intensification of the southern hemisphere atmospheric westerly jet over the latter part of the 20th century (e.g., Swart and Fyfe 2012, Thomas et al. 2015). This is also the case for the CMIP6 historical simulations, where in nearly all models there is an increase and poleward shift in the peak wind stress in the southern hemisphere, which results in an increase in the wind stress curl between 40-60 °S and a decrease north and south of this region, see **Fig 6a**.

Numerous modeling studies have shown that a shift and/or intensification of the southern westerlies causes substantial changes in the ocean circulation, transport, and tracer (including ideal age) distributions (e.g., Gent and Danabasoglu 2011, Sijp and England 2008, Farneti and Gent 2011, Waugh et al. 2019, 2021, Couldrey et al. 2021). Specifically, Waugh et al. (2019) show that a poleward shift of the winds produces an increase in age around 35 ^{o}S, qualitatively similar to the change in AOU or age in the CMIP6 historical simulations (see figure 3 of Waugh et al. 2019). This wind shift also causes a decrease in T and S in the same region (e.g. Sijp and England 2008), again consistent with the CMIP6 simulations.

Waugh et al. (2019) linked the age response to the vertical movement of isopycnals and changes in the subtropical gyres: For a poleward shift in winds there is decreased wind stress curl in the subtropics, which results in upward movement of isopycnal (Ekman suction) and poleward shift of subtropical gyre (Sverdrup balance), which both contribute to an increase in age around 30 ^{o}S. The CMIP6 simulations show an increase in density in the subtropics between 500 and 1500 m, consistent with a decrease in the wind stress curl, and reverse at high latitudes (**Fig. 6b**). Furthermore, the region of increasing density in the subtropics is similar to the region with increasing AOU and age (**Fig. 4** and **5)**. This supports the hypothesis that the decrease in wind stress over the subtropics leads to anomalous upwelling in the subtropics, which increases the age and AOU (by moving up older water).

As noted above, Waugh et al. (2019) also connected changes in age to changes in the subtropical gyres. Specifically, a poleward shift of peak wind stress leads to a poleward shift of the equatorward edge of the subtropical gyre (assuming Sverdrup balance), which results in older ages in the subtropics as there is reduced ventilation by subtropical gyre circulation (and hence a larger contribution from vertical mixing with deep waters). The patterns of change in CMIP6 multi-model age and AOU are consistent with this proposed mechanism, with largest increases near the equatorward edge of the gyres, see **Fig. 7a,b.**

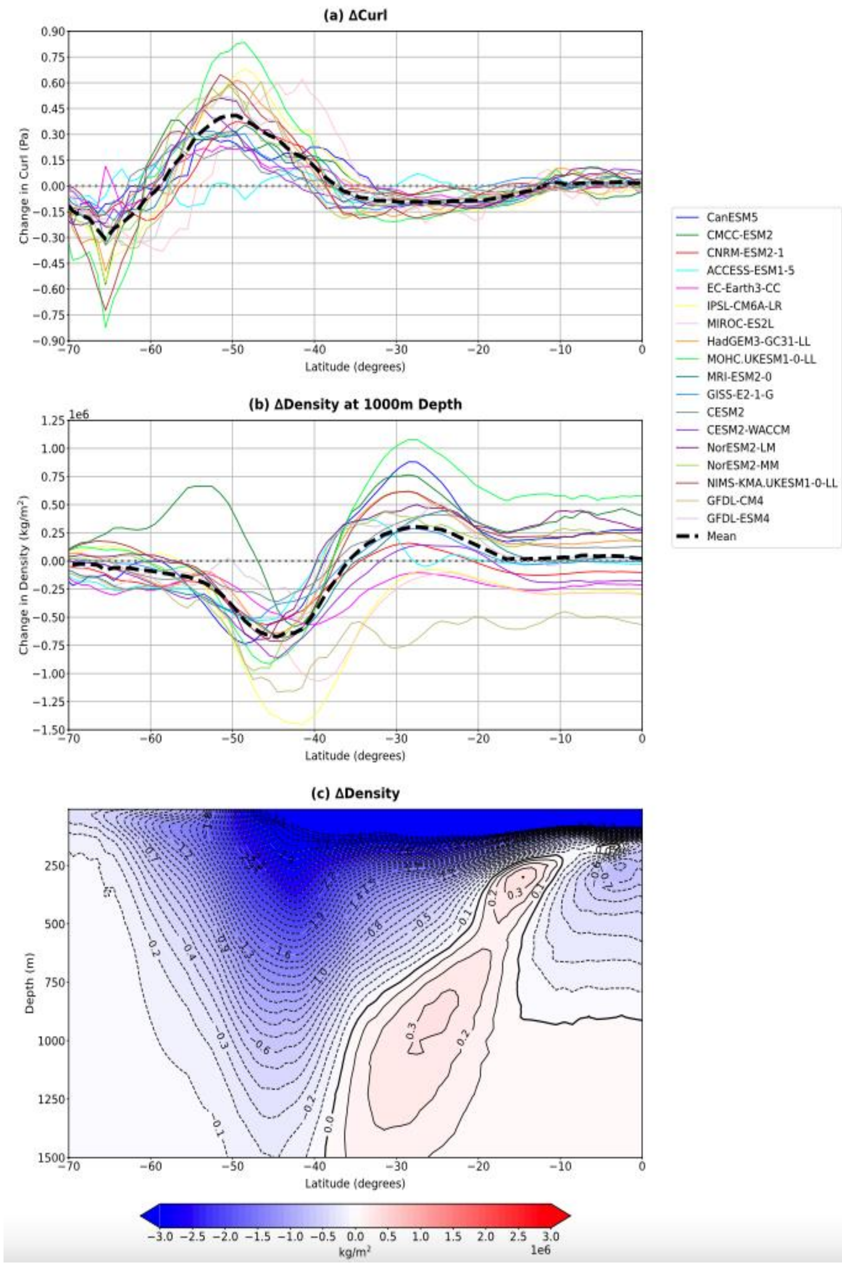

Figure 6: (a) Change in (a) wind stress curl and (b) density at 1000 m for each model and multi-model mean (black dashed curve), and (c) depth-latitude variations in multi-model mean historical change in density.

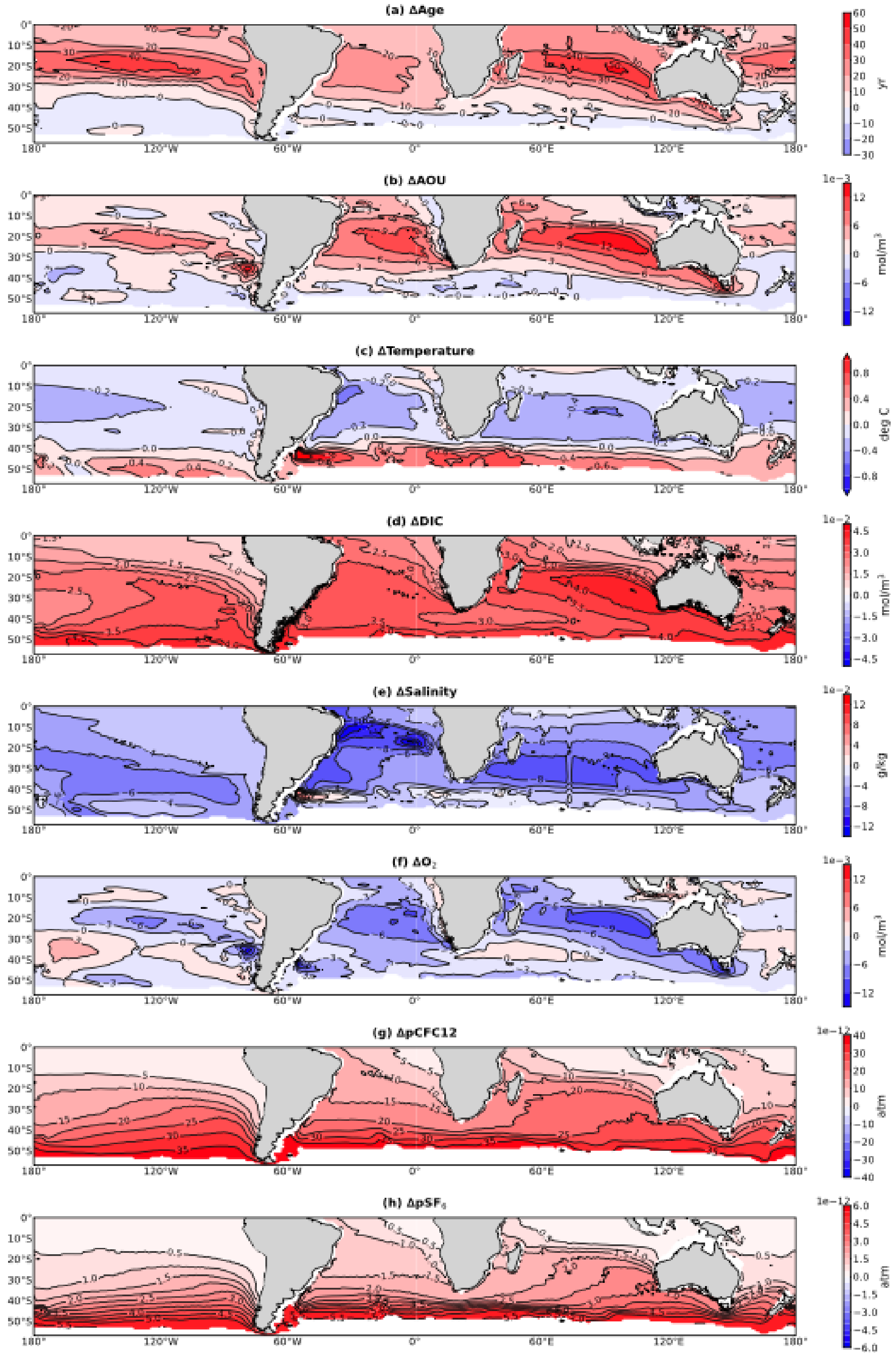

Figure 7: Maps of the multi-model (a) Δage, (b) ΔAOU, (c) ΔT, (d) ΔS, (e) ΔO_2, (f) ΔDIC, (g) ΔpCFC12, and (h) ΔpSF_6 interpolated on to the σ_2=35.5 kg/m^3 isopycnal surface for the last 20 years.

The changes in other tracers in the CMIP6 simulations are also consistent with above mechanisms. The sign and magnitude of the impact of the movement of isopycnals and ventilated gyre will depend on the tracer gradients, e.g., anomalous upwelling will lead to a decrease in tracer concentration if the tracer concentration decreases with depth. T, S, and O_2 decrease with depth (between 100 and 1000m) in the southern subtropics (**Fig. 8b-d**), and an upward movement of isopycnals would decrease T, S, and O_2 in this region. In contrast, DIC has a very weak vertical gradients in this region (**Fig. 8a**), and changes in upwelling will have limited impact on DIC. Similar arguments hold for horizontal gradients in the tropics and poleward movement of the gyre circulation.

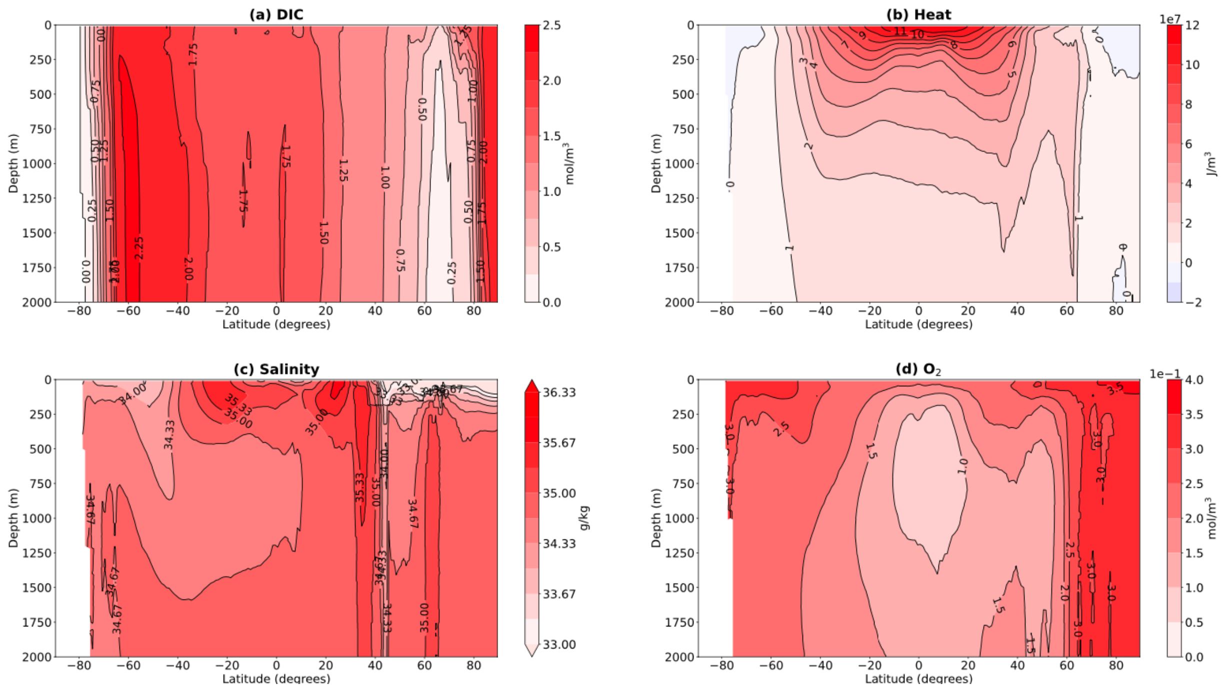

Figure 8: Depth-latitude variations in multi-model mean zonally-averaged (a) DIC, (b) Heat, (c) Salinity, and (d) O_2, for the first 20 years of the historical simulations. There is no CFC12 and SF_6 in the oceans during this period.

While not the total cause, the above connections to the change in wind stress could explain some of the large spread in ΔH, ΔS, and ΔO_2 among the models. There is a large spread in the strength and the meridional shift in the southern westerlies among the models (as is the case for CMIP5 simulations, e.g., Swart and Fyfe 2012, Thomas et al., 2015) which results in a spread in wind stress curl (**Fig. 6a)**, and then a spread in the change in density (**Fig. 6b**). This will then, by the above mechanisms involving the subtropical gyre and Ekman pumping, result in a spread in the transport driven change in tracers.

5. Conclusions

Examination of CMIP6 historical simulations shows substantial pre-industrial to present-day changes in multiple physical and biogeochemical ocean tracers. There are, however, differences among the tracers in both the spatial structure of the changes and the consistency in trends among models. The tracers can be separated into two groups. DIC, CFC12, and SF_6 all increase through the thermocline, with largest increases near the surface and very weak changes below the thermocline, and there is general agreement amongst the models. In contrast, the sign of the change in H, S, and O_2 varies between regions, with largest changes not necessarily at the surface, and there are large differences between models.

We suggest that the differences between the two groups is related to differences in the relative role of transport of time-varying surface values into the interior by a steady ocean circulation (the "added" component) compared with changes due to climate-driven changes in the ocean circulation (the "redistributed" component). The changes in the first group are dominated by the "added" component, whereas the "redistributed" component plays a significant role for the second group (at least in some regions). This importance of redistribution has been suggested previously to explain the differences between carbon and heat uptake (e.g., Winton et al. 2013, Bronselaer and Zanna 2020, Williams et al. 2021), but as shown here this can also explain differences in the changes in other ocean tracers.

The climate-driven changes in the ocean circulation produce changes in the ventilation time of waters, with the largest change occurring in the southern subtropics, where there is an increase in AOU and the ideal age tracer. This increase in age in the southern subtropics is, at least partially, driven by a poleward shift of the southern hemisphere westerly winds in the historical simulations. This results in a decrease in the subtropical wind stress curl, increased upwelling, and a poleward shift of subtropical gyre in the subtropics. This results in a negative ΔH, ΔS and ΔO_2 but only small changes in DIC because of differences in the sign and magnitude of vertical and meridional gradients of the tracers (**Fig. 8**). The large model spread in southern wind stress trends likely contributes to a large spread in circulation changes, and hence spread in ΔH, ΔS, and ΔO_2.

There are several aspects that require further investigation. We have focused here on zonally integrated properties, and there is a need to examine zonal variations and whether the same grouping of tracers applies in different regions (basins). Preliminary analysis indicates that the same general conclusions apply to all three basins in the southern hemisphere, although there are differences in magnitude and location of peak changes between basins, see, e.g., **Fig. 7.** This analysis could also further examine the cause of the changes, and connections to wind changes (which vary between oceans, e.g. Waugh et al. 2020).

There also needs to be further examination of the large differences in circulation changes, and hence tracer redistribution, between models. While this could be due to fundamental differences between models it could also be due to large internal variability. It thus will be of interest to examine the wind stress and ocean tracer changes in large ensembles performed by single climate models (e.g., Kay et al. 2015). How does the spread in wind trends and tracer fields within this single model ensemble compare with the multi-model ensemble, and is there a relationship between wind and tracer trends (i.e. does the spread in wind trends explain the spread in ocean tracer trends)?

Finally, an obvious area that needs investigation is comparisons with the observed changes in the different fields. One question to be answered includes whether the similarity in ΔH, ΔS, and ΔO_2, and their connections with changes in wind stress, heave, and age, is observed. Also, given the large model spread in these trends, a second question is which of the models are most realistic. A detailed analysis of the observed ocean changes and possible connections with wind changes is left for future work. However, it is worth noting that published studies of observed changes show features broadly consistent with multi-model mean results. Specifically, trends (since 1960) in observed temperature and salinity show decreases in both fields in the southern subtropical subsurface, but an increase in temperature and (small) decrease in salinity at higher southern latitudes (e.g. fig 2 of Cheng et al (2022) and fig 6 of Cheng et al. (2020)). A more detailed model-data comparison of these fields, as well as with available O_2, DIC, and transient tracer data, is needed. The analysis here suggests that such a multi-tracer approach could provide insights into the relative role of addition and redistribution of tracers in the ocean.

Acknowledgments

We acknowledge the World Climate Research Programme, which, through its Working Group on Coupled Modelling, coordinated and promoted CMIP6. We thank the climate modeling groups for producing and making available their model output, the Earth System Grid Federation (ESGF) for archiving the data and providing access, and the multiple funding agencies who support CMIP6 and ESGF.

Open Research

The CMIP6 data are publicly available from the Earth System Grid Federation archive https://esgf-node.llnl.gov/search/cmip6/.

References

Bahl, A., Gnanadesikan, A., & Pradal, M. A. (2019). Variations in ocean deoxygenation across earth system models: isolating the role of parameterized lateral mixing. *Global Biogeochemical Cycles*, 33(6), 703-724

Banks, H. T., and J. M. Gregory (2006). Mechanisms of ocean heat uptake in a coupled climate model and the implications for tracer based predictions of ocean heat uptake, *Geophys. Res. Lett.*, 33, L07608, doi:10.1029/ 2005GL025352.

Breitburg, D., Levin, L.A., Oschlies, A., Grégoire, M., Chavez, F.P., Conley, D.J., Garçon, V., Gilbert, D., Gutiérrez, D., Isensee, K. and Jacinto, G.S. (2018). Declining oxygen in the global ocean and coastal waters. *Science*, 359(6371), p.eaam7240

Bronselaer B, Zanna L. (2020). Heat and carbon coupling reveals ocean warming due to circulation changes. *Nature* 584:227–33

Cheng, L., Trenberth, K.E., Gruber, N., Abraham, J.P., Fasullo, J.T., Li, G., Mann, M.E., Zhao, X. and Zhu, J. (2020). Improved estimates of changes in upper ocean salinity and the hydrological cycle. *Journal of Climate*, 33(23), pp.10357-10381.

Cheng, L., von Schuckmann, K., Abraham, J.P., Trenberth, K.E., Mann, M.E., Zanna, L., England, M.H., Zika, J.D., Fasullo, J.T., Yu, Y. and Pan, Y., 2022. Past and future ocean warming. *Nature Reviews Earth & Environment*, pp.1-1

Clément, L., McDonagh, E.L., Gregory, J.M., Wu, Q., Marzocchi, A., Zika, J.D. and Nurser, A.J.G. (2022). Mechanisms of ocean heat uptake along and across isopycnals. *Journal of Climate*, 35(15), 4885-4904

Couldrey, M. P., et al. (2021). What causes the spread of model projections of ocean dynamic sea-level change in response to greenhouse gas forcing? *Climate Dyn.*, 56, 155–187, https://doi.org/10.1007/s00382-020-05471-4.

Durack, P. J. (2015). Ocean salinity and the global water cycle. *Oceanography*, 28, 20–31.

England, M. H. (1995). The age of water and ventilation timescales in a global ocean model. *Journal of Physical Oceanography*, *25*(11), 2756–2777

Eyring, V., Bony, S., Meehl, G.A., Senior, C.A., Stevens, B., Stouffer, R.J. and Taylor, K.E. (2016). Overview of the Coupled Model Intercomparison Project Phase 6 (CMIP6) experimental design and organization. *Geoscientific Model Development*, *9*(5), pp.1937-1958.

Gruber, N., Bakker, D.C., DeVries, T., Gregor, L., Hauck, J., Landschützer, P., McKinley, G.A. and Müller, J.D. (2023). Trends and variability in the ocean carbon sink. *Nature Reviews Earth & Environment*, pp.1-16

Farneti, R. and Gent, P.R. (2011). The effects of the eddy-induced advection coefficient in a coarse-resolution coupled climate model. *Ocean Modelling*, 39, 135-145

Frölicher, T. L., Sarmiento, J. L., Paynter, D. J., Dunne, J. P., Krasting, J. P., and Winton, M. (2015). Dominance of the Southern Ocean in Anthropogenic Carbon and Heat Uptake in CMIP5 Models. J. Climate, 28(2), 862–886, doi: 10.1175/JCLI-D-14-00117.1.

Gent, P.R., and G. Danabasoglu (2011). Response to Increasing Southern Hemisphere Winds in CCSM4, *J. Climate*, 4992-4998.

Hall, T.M. and Haine, T.W. (2002. On ocean transport diagnostics: The idealized age tracer and the age spectrum. *Journal of physical oceanography*, *32*(6), pp.1987-1991.

Johnson, G., Lyman, J., Boyer, T., Cheng, L., Domingues, C., Gilson, J., et al. (2018). Ocean heat content [in State of the Climate in 2017]. *B. Am. Meteorol. Soc*. 99, S72–S77. doi: 10.1175/2018BAMSStateoftheClimate.1

Kay, J. E., Deser, C., Phillips, A., Mai, A., Hannay, C., Strand, G., Arblaster, J., Bates, S., Danabasoglu, G., Edwards, J., Holland, M. Kushner, P., Lamarque, J.-F., Lawrence, D., Lindsay, K., Middleton, A., Munoz, E., Neale, R., Oleson, K., Polvani, L., and M. Vertenstein (2015). The Community Earth System Model (CESM) Large Ensemble Project: A Community Resource for Studying Climate Change in the Presence of Internal Climate Variability, *Bull. Amer. Meteorol.* Soc., 96, 1333-1349

Keeling, R.F., Körtzinger, A. and Gruber, N. (2010). Ocean deoxygenation in a warming world. *Annual review of marine science*, 2, pp.199-229.

Marinov, I., & Gnanadesikan, A. 2011. Changes in ocean circulation and carbon storage are decoupled from air-sea CO 2 fluxes. *Biogeosciences*, 8(2), 505-513.

McKinley, G.A., Fay, A.R., Lovenduski, N.S. and Pilcher, D.J. (2017). Natural variability and anthropogenic trends in the ocean carbon sink. *Annual review of marine science*, 9, pp.125-150

Newsom, E., Zanna, L. and Khatiwala, S. (2022). Relating patterns of added and redistributed ocean warming. *Journal of Climate*, 35(14), pp.4627-4643

Sijp, W. P., and M. H. England (2008). The effect of a northward shift in the southern hemisphere westerlies on the global ocean. *Prog. Oceanogr*., 79, 1–19, https://doi.org/10.1016/ j.pocean.2008.07.002.

Swart, N. C., and J. C. Fyfe (2012). Observed and simulated changes in the Southern Hemisphere surface westerly wind-stress, Geophys. Res. Lett., 39, L16711, doi:10.1029/2012GL052810.

Thiele, G. and Sarmiento, J.L., (1990). Tracer dating and ocean ventilation. *Journal of Geophysical Research: Oceans*, 95(C6), pp.9377-9391.

Thomas, J. L., D. W. Waugh, and A. Gnanadesikan (2015). Southern Hemisphere extratropical circulation: Recent trends and natural variability, *Geophys. Res. Lett*., 42, doi:10.1002/2015GL064521.

Walker, S. J., Weiss, R. F., and Salameh, P. K. (2000). Reconstructed histories of the annual mean atmospheric mole fractions for the halocarbons CFC-11 CFC-12, CFC-113, and carbon tetrachloride, *J. Geophys. Res.*, 105(C6), 14285– 14296, doi:10.1029/1999JC900273.

Waugh, D.W., A. McC. Hogg, P Spence, M. H. England, T. W.N. Haine (2019). Response of Southern Ocean ventilation to changes in mid-latitude westerly winds, *J. Climate*, 32, 5345-5361.

Waugh, D. W., Banerjee, A., Fyfe, J. C., and Polvani, L. M. (2020). Contrasting recent trends in Southern Hemisphere westerlies across different ocean basin. *Geophys. Res. Lett.*, 47, e2020GL088890

Waugh, D. W., Stewart, K., Hogg, A. M., and England, M. H. (2021). Interbasin differences in ocean ventilation in response to variations in the Southern Annular Mode. *J. Geophys. Res.: Oceans*, 126, e2020JC016540.

Williams, R.G., Katavouta, A. and Roussenov, V. (2021). Regional asymmetries in ocean heat and carbon storage due to dynamic redistribution in climate model projections. *J. Climate*, 34(10), pp.3907-3925.

Winton, M., S. M. Griffies, B. L. Samuels, J. L. Sarmiento, and T. L. Frölicher (2013). Connecting changing ocean circulation with changing climate. *J. Climate*, 26, 2268–2278